1999

Mon. Not. R. Astron. Soc. **000**, 1–12 (1999)

Detection of new sources of methanol emission at 107 and 108 GHz with the Mopra telescope

I.E. Val'tts,[1] S.P. Ellingsen,[2] V.I. Slysh,[1] S.V. Kalenskii,[1] R. Otrupcek[3] and M.A. Voronk
[1] *Astro Space Center of Lebedev Physical Institute, Profsoyuznaya 84/32, 117810 Moscow, Russia*
[2] *School of Mathematics and Physics, University of Tasmania, GPO Box 252-21, Hobart 7001, TAS, Australia*
[3] *Australia Telescope National Facility, PO Box 76, Epping 2121, NSW, Australia*

Received date; accepted date

ABSTRACT
A southern hemisphere survey of methanol emission sources in two millimeter wave transitions has been carried out using the ATNF Mopra millimetre telescope. Sixteen emission sources have been detected in the $3_1-4_0A^+$ transition of methanol at 107 GHz, including six new sources exhibiting class II methanol maser emission features. Combining these results with the similar northern hemisphere survey, a total of eleven 107-GHz methanol masers have been detected. A survey of the methanol emission in the $0_0-1_{-1}E$ transition at 108 GHz resulted in the detection of 16 sources; one of them showing maser characteristics. This is the first methanol maser detected at 108 GHz, presumably of class II. The results of LVG statistical equilibrium calculations confirm the classification of these new sources as a class II methanol masers.

Key words: ISM: radio lines: ISM – masers – surveys – ISM: molecules

1 INTRODUCTION

Methanol masers are found in star forming regions, which manifest themselves as infrared sources, molecular outflows and compact HII regions. They are divided into two classes, I and II (Batrla et al. 1987; Menten 1991a). Class I methanol masers are not directly associated with any known physical object, but are located in general regions of star formation. By contrast, class II methanol masers are usually observed in the vicinity of newly formed luminous stars, and are closely related to ultracompact HII regions and OH masers. Both class I and II methanol masers typically emit in several transitions. Figs. 1 and 2 show energy level diagrams, separately for A and E-methanol. In A-methanol masers occur mostly in transitions between K=1 and K=0 ladders, with class I maser transitions having their upper energy level in the K=0 ladder and class II maser transitions having their upper energy level in the K=1 ladder. In E-methanol most maser transitions occur between K=0 and K=−1 ladders, with class I maser transitions having their upper energy level in the K=−1 ladder and class II maser transitions having their upper energy level in the K=0 ladder.

The strongest methanol masers are the class II masers from the $5_1 - 6_0A^+$ transition at 6.7 GHz (Menten 1991b) and the $2_0 - 3_{-1}E$ transition at 12.2 GHz (Batrla et al. 1987). Weaker class II methanol masers have been detected at millimeter wavelengths from the $J_0 - J_{-1}E$ transitions at 157 GHz (Slysh, Kalenskii & Val'tts 1995). Another millimeter methanol maser line from the $3_1 - 4_0A^+$ transition at 107 GHz (shown by the arrow in Fig. 1) was discovered at Onsala (Sweden) (Val'tts et al. 1995). Val'tts et al. detected five 107-GHz methanol maser sources, all in the northern hemisphere. Two of them – Cep A and W3(OH) – have been mapped with high angular resolution using BIMA (Mehringer, Zhou & Dickel 1997; Slysh et al. 1999a). The masers are unresolved by BIMA, yielding a lower limit on the brightness temperature at 107 GHz of 5×10^5K in W3(OH).

To date the only published search for 107-GHz methanol masers is that by Val'tts et al. (1995). In this paper we present the results of an extensive search for 107-GHz methanol emission in the southern hemisphere with the Mopra 22-m telescope (Australia). These observations complement the northern hemisphere survey of Val'tts et al. and completes a search for 107-GHz methanol maser emission toward sources which show strong 6.7-GHz maser emission. A survey of methanol emission in the $0_0-1_{-1}E$ transition (shown by the arrow in Fig. 2) at 108 GHz was also performed, this represents the first search for maser emission from this transition.

2 OBSERVATIONS

The sources searched for methanol emission at 107 and 108 GHz were selected from 6.7-GHz methanol masers detected by Menten (1991b), Schutte et al. (1993), Caswell et al. (1995a), van der Walt et al. (1995) and Slysh et al.

(1999b). This included all 6.7-GHz methanol masers with a peak flux density greater than 50 Jy south of declination +21.

The observations were carried out in the period from July 1 to 17, 1997, using the Mopra 22-m millimeter-wave telescope of the ATNF. The assumed rest frequencies of the $3_1 - 4_0 A^+$ and $0_0 - 1_{-1} E$ transitions of methanol were 107.01367 GHz (Val'tts et al. 1995) and 108.893940 GHz (De Lucia et al. 1989) respectively. At these frequencies only the inner 15 metres of the Mopra antenna is illuminated and the aperture efficiency is 41%, which implies that one Kelvin of antenna temperature corresponds to 40 Jy for both frequencies. The half-power beamwidth at 107 and 108.9 GHz is 46and 455, respectively. The antenna pointing was checked every 12 hours through observations of 86-GHz SiO masers, the pointing accuracy of the Mopra antenna is 10 rms. The observations were performed in a position switching mode with reference positions offset 30.

A cryogenically cooled low-noise SIS mixer was used in the receiver. For the 107-GHz observations the single side-band receiver noise temperature was 140 K and the system temperature varied between 240 K and 325 K depending on weather conditions and the elevation of the telescope, while at 108 GHz the single side-band receiver noise temperature was 160 K and the system temperature varied between 255 K and 400 K. An ambient temperature load (assumed to have a temperature of 290K) was regularly placed in front of the receiver to enable calibration using the method of Kutner & Ulich (1981), this corrects the observed flux density for the effects of atmospheric absorption. Variations in the ambient temperature of a few percent occurred during the observations, and the estimated uncertainty of the absolute flux density scale is 10%.

The back-end was a 64 MHz wide 1024-channel autocorrelator with a frequency resolution of 62.5 kHz. This yielded a velocity resolution at 107 GHz of 0.210 km s^{-1} with uniform weighting and 0.350 km s^{-1} with Hanning smoothing. At 108 GHz the velocity resolution was 0.207 km s^{-1} with uniform weighting and 0.344 km s^{-1} with Hanning smoothing. For each source a uniformly weighted spectrum was produced with a velocity range of approximately 70 km s^{-1} centred on the velocity of the observed 6.7 and 12.2-GHz methanol maser, or CS thermal emission. The spectrum was then Hanning smoothed, as many of the sources are weak this usually improved the signal to noise ratio. The spectra and Gaussian parameters (peak flux density, velocity and full width half maximum) in all figures and tables are Hanning smoothed data unless otherwise noted.

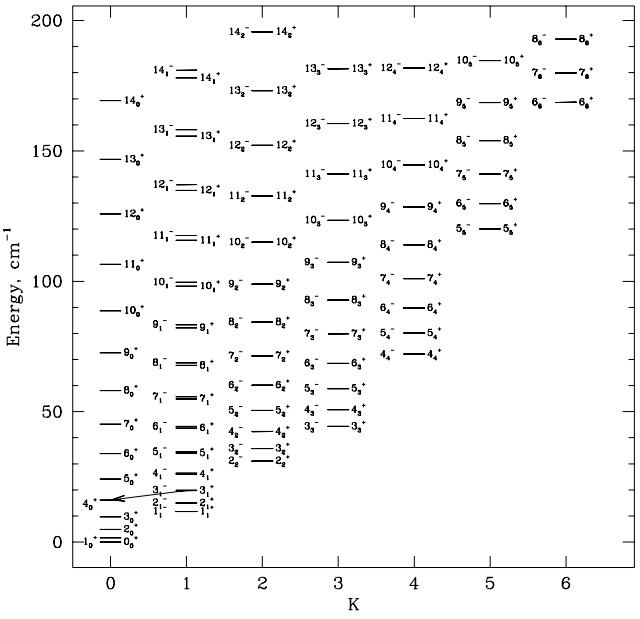

Figure 1. Energy levels for A-methanol species. The arrow represents the 107-GHz transition

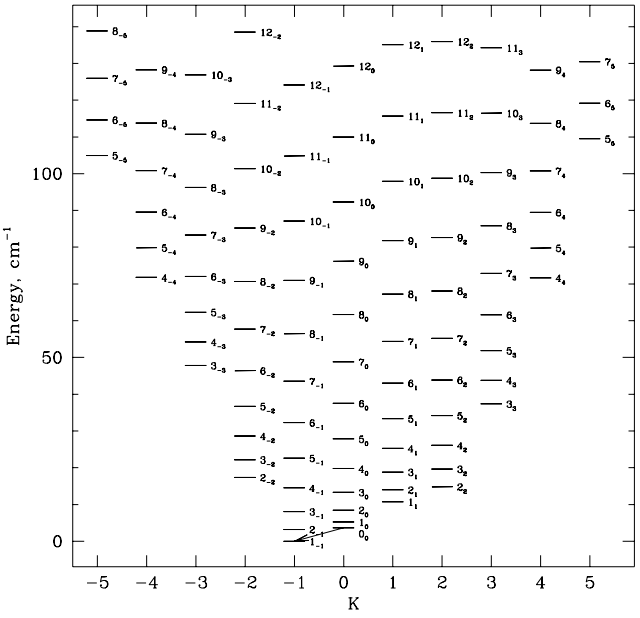

Figure 2. Energy levels for E-methanol species. The arrow represents the 108-GHz transition

3 RESULTS

Emission from the 107-GHz transition of methanol was detected in 16 of the 79 sources observed. The detected sources are listed in Table 1 with the Gaussian parameters of spectral features. Their spectra are shown in Fig. 3. Non-detections are given in Table 2. The detection limit after Hanning smoothing the spectra varied between 3 and 8 Jy at the 3$-\sigma$ level.

Five sources from Table 1 were discovered previously by Val'tts et al. (1995) at Onsala. At 107 GHz there is a rather good agreement in the radial velocity and line width of the

Table 1. Detected 107-GHz methanol sources. Gaussian parameters were determined from Hanning smoothed spectra, except for Orion KL, 328.81+0.63, 339.88-1.26 and 345.01+1.79

Source	R.A. 1950 (h m s)	Dec. 1950 (°)	Peak Flux Density (Jy)	LSR radial velocity (km s^{-1})	Line FWHM (km s^{-1})
Orion S6	05 32 44.8	−05 26 00.0	8.9(0.6)	6.5(0.1)	3.9(0.3)
Orion KL	05 32 47.0	−05 24 23.0	29.3(7.3)	7.4(0.1)	1.7(0.4)
			40.0(5.5)	7.6(0.2)	5.2(0.5)
S252	06 05 54.0	+21 39 09.0	7.2(1.0)	10.3(0.1)	0.8(0.1)
305.208+0.206	13 08 01.6	−62 18 44.8	3.7(0.4)	−40.4(0.3)	2.5(0.7)
IRAS13484−6100	13 48 24.4	−61 01 30.0	4.4(0.5)	−55.8(0.1)	2.1(0.3)
323.74−0.26	15 27 52.0	−56 20 39.5	4.7(0.7)	−53.2(0.2)	1.6(0.3)
			14.5(0.5)	−50.8(0.1)	2.4(0.1)
328.81+0.63	15 52 00.3	−52 34 22.2	10.6(1.4)	−44.1(0.1)	0.6(0.1)
			13.1(0.5)	−42.1(0.1)	6.0(0.2)
337.403−0.400	16 35 07.9	−47 22 04.1	10.9(0.5)	−40.8(0.1)	4.4(0.2)
339.88−1.26	16 48 24.8	−46 03 33.9	58.7(4.3)	−38.8(0.1)	0.8(0.1)
			49.6(1.5)	−37.6(0.1)	1.5(0.1)
			29.3(5.5)	−36.1(0.1)	0.4(0.1)
			19.1(2.9)	−35.3(0.1)	1.0(0.4)
			67.8(2.4)	−34.2(0.1)	1.1(0.1)
345.01+1.79	16 53 19.7	−40 09 46.0	84.5(2.4)	−22.3(0.1)	1.1(0.1)
NGC6334F	17 17 32.4	−35 44 04.2	18.4(3.3)	−10.6(0.1)	2.5(0.4)
			12.2(1.7)	−7.7(0.4)	3.5(0.6)
351.78−0.54	17 23 20.7	−36 06 45.5	5.4(0.3)	−3.1(0.2)	8.1(0.6)
Sgr A−G	17 42 27.3	−29 04 35.8	9.6(1.7)	19.5(0.1)	0.4(0.2)
Sgr B2	17 44 10.7	−28 22 17.0	16.6(1.1)	57.5(0.7)	19.0(1.5)
9.62+0.20	18 03 16.0	−20 31 52.0	13.9(1.1)	−1.0(0.1)	1.0(0.1)
			3.8(0.4)	1.2(0.4)	6.4(0.8)
W48	18 59 13.1	+01 09 07.0	9.2(1.3)	41.1(0.2)	1.7(0.4)
			8.0(1.8)	44.3(0.1)	2.0(0.2)

spectral features observed at Mopra and Onsala. The flux densities do not agree so well. In Orion S6 and 9.62+0.20 the flux densities, measured at Mopra are a factor of two larger than the Onsala flux densities (see Fig. 4). On the other hand, the S252 and W48 flux densities, measured at Mopra are a factor of 1.5 less than those observed at Onsala. These differences are most likely due to a combination of calibration and pointing errors and poor signal-to-noise ratios. For 9.62+0.20 the inconsistency may be due to the difference in spectral resolution, or possible variability during the time interval of 4.2 years between the two sets of observations. Ten sources from Table 1 have also been observed at SEST by Booth & Caswell (private communication). Some of our undetected sources were found at SEST with better sensitivity. The sources detected at SEST but not at Mopra are MonR2, 309.92+0.48, 338.92+0.55, 340.78-0.10, 345.00-0.22 and W33B (Booth & Caswell, private communication).

Emission was detected toward 16 of the 41 source observed at 108 GHz. The Gaussian parameters of the detected sources are listed in Table 3 and their spectra are shown in Fig. 5. The list of non-detections is given in Table 4. The detection limit varied between 3 and 7 Jy at the $3-\sigma$ level.

Three objects from Table 3 have also been observed at 108 GHz with the 30-m telescope at Pico Veleta: Orion KL, 345.01+1.79 and 9.62+0.20 (Slysh et al. 1999c). Similar to the comparison of 107-GHz sources between Mopra and Onsala observations, at 108 GHz there is rather good agreement in the radial velocity and line width of spectral features observed at Mopra and at Pico Veleta, but the flux densities differ significantly. There is a difference between Orion KL flux densities (see Fig. 6); which is probably due to poor weather during the observations of Orion KL at Pico Veleta, which resulted in large calibration errors. The flux densities of the other sources are in reasonable agreement. Four sources from the list of those undetected at Mopra at 108 GHz (Table 4) were also observed at Pico Veleta. Two of them, M8E and 35.20-0.74 were detected there, however, S252 and W48 were not. The detection of M8E and 35.20-0.74 at Pico Veleta and non-detection in Mopra is consistent with a higher sensitivity at Pico Veleta.

3.1 Comments on detected maser sources

Some of the newly detected sources show narrow lines with full width half maximum (FWHM) of 1-2 km s^{-1} or less. This line width is less than that of thermal lines toward these sources and suggests that the emission is of maser origin. Another indicator of maser emission is its anomalously high intensity; this can be seen from the comparison of intensities at 107 and 108 GHz. In thermal emission sources the intensity at the two frequencies is equal to within a factor of two or three. In maser sources the difference between

Table 2. Sources undetected at 107 GHz (all spectra Hanning smoothed).

Source	R.A. 1950 (h m s)	Dec. 1950 (° ′ ″)	LSR radial velocity (km s^{-1})	RMS (Jy)
IRAS05329−0512	05 32 58.7	−05 12 11.0	11.1	1.8
L1641N	05 33 52.7	−06 54 02.0	7.2	1.5
Mon R2	06 05 20.0	−06 22 40.0	12.0	1.2
S269	06 11 47.1	+13 50 34.0	15.0	2.1
IRAS07077−1026	07 07 43.6	−10 26 47.9	13.7	1.6
IRAS08076−3556	08 07 40.1	−35 56 07.6	5.9	1.6
IRAS08448−4343	08 44 49.3	−43 43 28.0	3.7	1.5
IRAS08470−4243	08 47 00.5	−42 43 15.0	12.3	1.6
IRAS09002−4732	09 00 12.2	−47 32 06.5	3.1	1.5
IRAS09018−4816	09 01 51.7	−48 16 41.7	10.3	1.6
IRAS09149−4743	09 07 42.2	−48 53 13.2	9.3	1.5
IRAS10184−5748	10 18 26.3	−57 48 31.5	8.9	1.6
IRAS10460−5811	10 46 03.4	−58 10 58.0	−1.8	1.7
305.21+0.21	13 08 01.7	−62 18 45.3	−38.0	1.2
309.921+0.479	13 47 11.8	−61 20 18.7	−59.6	1.4
IRAS14164−6028	14 16 24.4	−60 28 55.0	−47.8	1.7
318.95−0.20	14 57 03.8	−58 47 01.2	−34.7	1.5
IRAS15122−5801	15 12 02.6	−58 00 50.0	−62.0	1.4
IRAS15394−5358	15 39 28.4	−53 58 28.0	−38.0	1.3
IRAS15408−5356	15 40 45.8	−53 56 28.0	−43.0	1.3
IRAS16019−4903	16 02 03.2	−49 04 14.0	−23.6	1.1
331.28−0.19	16 07 38.0	−51 34 12.4	−78.0	1.2
IRAS16084−5127	16 08 24.0	−51 27 15.0	−86.0	1.4
331.45−0.18	16 08 26.2	−51 26 57.4	−88.5	1.3
333.129−0.429	16 17 13.4	−50 28 12.5	−51.2	1.9
333.58−0.02	16 17 28.0	−49 51 42.7	−35.9	1.2
333.45−0.18	16 17 32.3	−50 04 08.0	−42.5	1.2
333.47−0.17	16 17 34.7	−50 02 45.0	−42.0	1.2
332.96−0.68	16 17 35.2	−50 45 56.3	−45.9	1.3
334.65−0.02	16 25 51.1	−49 13 07.0	−30.1	1.1
335.79+0.17	16 26 04.7	−48 09 20.4	−47.5	1.1
336.022−0.819	16 31 21.8	−48 40 51.0	−53.2	1.3
336.83−0.36	16 36 22.2	−47 51 48.0	−22.7	2.0
338.92+0.55	16 36 54.8	−45 36 14.0	−62.0	1.6
339.62−0.12	16 42 26.5	−45 31 18.0	−36.0	1.9
340.785−0.096	16 46 38.2	−44 37 18.6	−107.0	1.4
339.68−1.21	16 47 25.0	−46 10 59.0	−21.0	1.9
341.22−0.21	16 48 42.1	−44 21 53.0	−38.0	1.2
345.00−0.22	17 01 38.5	−41 24 59.0	−22.0	1.9
345.400−0.941	17 05 59.8	−41 32 07.0	−20.9	1.9
350.504+0.956	17 13 40.2	−36 17 54.5	−10.3	2.0
352.630−0.567	17 25 49.8	−35 25 16.3	−0.4	2.1
351.633−1.252	17 25 53.6	−36 37 50.3	−11.9	2.1
IRAS17440−2824	17 44 04.8	−28 25 49.0	49.5	1.8
0.64−0.04	17 44 08.9	−28 23 29.0	49.0	1.7
0.54−0.85	17 47 04.1	−28 54 01.0	14.8	1.7
IRAS17480−2623	17 47 44.4	−26 38 52.0	3.0	2.2
IRAS17589−2312	17 58 56.2	−23 13 53.0	26.4	1.6
M8E	18 01 49.7	−24 26 56.0	10.8	1.5
11.90−0.14	18 05 15.2	−18 42 21.0	43.0	1.6
10.30−0.15	18 05 57.9	−20 06 26.0	10.6	1.2
IRAS18060−2005	18 06 06.7	−20 05 34.4	11.0	1.6
W33B	18 10 59.3	−18 02 40.0	30.0	1.3
IRAS18128−1640	18 12 51.1	−16 39 53.0	15.0	1.5
IRAS18134−1942	18 13 28.3	−19 42 25.0	6.7	1.6
L379IRS3	18 26 32.9	−15 17 58.0	18.0	1.4
IRAS18316−0602	18 31 38.9	−06 02 23.0	41.8	1.7
IRAS18353−0628	18 35 18.0	−06 28 00.0	95	1.8
25.72+0.01	18 35 29.2	−06 27 21.4	95.7	1.8

Source	R.A. 1950 (h m s)	Dec. 1950 (°)	LSR radial velocity (km s^{-1})	RMS (Jy)
W43M	18 45 37.2	−01 30 00.0	102.0	1.8
35.02+0.35	18 51 29.1	−01 57 26.0	44.0	1.7
IRAS18517+0437	18 51 48.7	+04 37 19.0	41.0	1.7
49.49−0.39	19 21 25.7	+14 24 42.0	59.0	2.0

Table 3. Detected 108-GHz methanol sources. Gaussian parameters were determined from Hanning smoothed spectra, except for Orion KL, 322.16+0.64, 328.81+0.63, 337.41-0.40, 345.01+1.79, NGC6334B and 351.77-0.54

Source	R.A. 1950 (h m s)	Dec. 1950 (°)	Peak Flux Density (Jy)	LSR radial velocity (km s^{-1})	Line FWHM (km s^{-1})
Orion S6	05 32 44.8	−05 26 00.0	6.4(0.5)	6.5(0.1)	4.1(0.3)
Orion KL	05 32 47.0	−05 24 23.0	19.4(0.7)	7.9(0.1)	4.4(0.2)
305.21+0.21	13 08 01.7	−62 18 45.3	5.7(0.5)	−41.1(0.2)	6.8(0.5)
318.95−0.20	14 57 03.8	−58 47 01.2	5.9(0.5)	−34.6(0.2)	3.8(0.4)
322.16+0.64	15 14 45.7	−56 27 28.0	12.7(0.7)	−57.1(0.1)	4.5(0.3)
328.81+0.63	15 52 00.3	−52 34 22.2	7.4(2.0)	−44.0(0.7)	9.4(1.0)
			11.4(2.0)	−41.8(0.2)	3.9(0.6)
337.41−0.40	16 35 09.8	−47 22 07.0	12.1(0.6)	−40.8(0.1)	4.9(0.3)
345.01+1.79	16 53 19.7	−40 09 46.0	7.5(1.2)	−22.1(0.1)	1.3(0.2)
			7.2(0.6)	−13.9(0.2)	4.6(0.4)
345.50+0.35	17 00 54.2	−40 40 18.0	3.7(0.5)	−18.0(0.2)	2.7(0.4)
345.00−0.22	17 01 38.5	−41 24 59.0	2.8(0.4)	−25.6(0.4)	3.9(0.8)
NGC6334B	17 16 35.5	−35 54 44.0	11.9(0.6)	−7.0(0.1)	4.7(0.3)
NGC6334C	17 16 54.5	−35 51 58.0	3.9(0.5)	−4.2(0.2)	3.6(0.5)
351.77−0.54	17 23 20.7	−36 06 45.4	11.8(0.5)	−3.2(0.1)	7.7(0.3)
9.62+0.20	18 03 16.0	−20 31 52.9	3.4(0.5)	4.1(0.3)	2.3(0.6)
W33A	18 11 43.8	−17 53 04.0	6.4(0.4)	36.2(0.2)	5.5(0.4)
49.49−0.39	19 21 25.7	+14 54 42.0	8.9(0.4)	56.8(0.2)	8.6(0.4)

the intensities at 107 and 108 GHz can be very large: for example, the peak flux density of the 107-GHz emission in 339.88−1.26 is at least ten times greater than that at 108 GHz. The overlap of several closely spaced narrow maser emission lines can produce a spectrum with an intense wide line, however, in such cases (e.g. 323.74−0.26) the intensity will be anomalously high. Based on these criteria we identify 9 sources in Table 1 as 107-GHz masers: S252, 323.74−0.26, 328.81+0.63, 339.88−1.26, 345.01+1.79, NGC6334F, Sgr A-G, 9.62+0.20, and W48. Below we give comments on some of the maser sources.

328.81+0.63. This source shows methanol maser emission at 6.7 GHz (Caswell et al. 1995a) and 12.2 GHz (Caswell et al. 1993; Caswell et al. 1995b), as well as in the class I $7_0 - 6_1 A^+$ transition at 44.1 GHz (Slysh et al. 1994). Hydroxyl masers at 1.665 and 6.035 GHz are also found here (Caswell, Haynes & Goss 1980; Smits 1994). The 107-GHz methanol spectrum (Fig. 3) shows a very narrow spike at −44.1 km s^{-1} and a broad component at −42.1 km s^{-1}. The narrow spike with a line width 0.6 km s^{-1} has the same radial velocity as the strongest component of 6.7-GHz maser, and must be a 107-GHz maser. At 108 GHz only a broad component is present. The broad components at 107 and 108 GHz correspond to thermal CS emission at V_{LSR}=−42.3 km s^{-1} (Bronfman, Nyman & May 1996).

339.88-1.26. The profile of the 107-GHz emission (Fig. 3) can be fitted by 5 narrow components with line widths between 0.4 and 1.5 km s^{-1} (see Table 1). The velocity range of the 107-GHz emission coincides with that of the 6.7-GHz methanol maser emission (Caswell et al. 1995a). Most of 107-GHz emission is clearly maser emission, no significant thermal emission is present. At 108 GHz the source was not detected, although thermal CS emission is present near the red edge of the 107-GHz emission velocity range (Bronfman et al. 1996).

345.01+1.79. This is a strong methanol maser at 6.7, 12.2 and 157 GHz (Caswell et al. 1995a; Norris et al. 1987; Slysh et al. 1995). At both 107 and 108 GHz there is a strong narrow maser component at the same velocity (−22 km s^{-1}) as the 6.7, 12.2, and 157-GHz masers. This is the only maser detected thus far at 108 GHz. A broad, probably thermal component at 108 GHz was found at the same velocity (−13.9 km s^{-1}) as thermal CS emission (Juvella 1996). For more detailed discussion of this source see Val'tts (1998).

9.62+0.20. This is the strongest methanol maser at 6.7 GHz (Menten 1991b). The 107-GHz maser was discovered at Onsala by Val'tts et al. (1995). At Mopra we found

Table 4. Sources undetected at 108 GHz (all spectra Hanning smoothed).

Source	R.A. 1950 (h m s)	Dec. 1950 (°)	LSR radial velocity (km s^{-1})	RMS (Jy)
Mon R2	06 05 20.0	−06 22 40.0	12.0	1.2
S252	06 05 53.5	+21 39 02.0	11.0	1.6
192.60−0.05	06 09 59.1	+18 00 10.0	5.0	1.5
S269	06 11 47.1	+13 50 34.0	15.0	2.0
IRAS08470−4243	08 47 00.5	−42 43 15.0	12.3	1.7
IRAS10460−5811	10 46 03.4	−58 10 58.0	−1.8	1.7
291.28−0.71	11 09 46.7	−61 02 06.0	−30.0	1.2
305.20+0.21	13 07 58.6	−62 16 42.3	−44.0	1.9
309.92+0.48	13 47 11.9	−61 20 18.8	−60.0	1.3
IRAS14164−6028	14 16 24.4	−60 28 55.0	−47.8	1.6
323.74−0.26	15 27 52.0	−56 20 39.5	−51.0	1.8
IRAS15539−5353	15 54 06.1	−53 50 47.0	−45.0	1.6
328.25−0.53	15 54 07.0	−53 49 25.0	−37.0	1.9
336.022−0.819	16 31 21.8	−48 40 51.0	−53.2	1.9
339.88−1.26	16 48 24.8	−46 03 33.9	−39.0	1.8
354.61+0.47	17 26 56.8	−32 41 34.0	−23.0	1.3
M8E	18 01 49.7	−24 26 56.0	10.0	2.4
8.68−0.37	18 03 22.6	−21 37 24.0	43.0	1.5
12.89+0.49	18 08 56.4	−17 32 14.0	39.0	1.5
W33B	18 10 59.3	−18 02 40.0	30.0	1.7
23.01+0.41	18 31 55.6	−09 03 09.0	75.0	1.7
25.72+0.01	18 38 10.4	−06 24 41.0	95.7	2.4
29.95−0.02	18 43 26.7	−02 42 38.0	96.0	2.2
35.20−0.74	18 55 41.1	+01 36 26.0	28.0	1.7
W48	18 59 13.1	+01 09 07.0	42.0	1.6

a narrow feature at −1 km s^{-1}, which differs from the radial velocity of the strongest 6.7-GHz feature (1 km s^{-1}), but there is weak 107-GHz emission at positive radial velocities (see Table 1 and Fig. 3). At 108 GHz there is only a weak broad feature at 4.1 km s^{-1}, close to the radial velocity of thermal CS emission 5 km s^{-1} (Larionov et al. 1999). We have already noted that the two spectra taken 4.2 years apart at Onsala and Mopra are different: the narrow peak became stronger by a factor of about 3 and its radial velocity changed by 0.5 km s^{-1}. If this is a real variability, it would be interesting to monitor the 107-GHz emission from this source.

W48. The 107-GHz methanol maser from this source was discovered at Onsala (Val'tts et al. 1995). The spectrum consists of two moderately narrow features as in other methanol transitions at 6.7 GHz (Menten 1991b) and 157 GHz (Slysh et al. 1995). At 108 GHz there is no detectable emission. The thermal CS line has a radial velocity of 43.6 km s^{-1} (Larionov et al. 1999), roughly coincident with the radial velocity of one of the methanol features 44.3 km s^{-1}.

4 DISCUSSION

The 107-GHz methanol masers detected in these and previous observations have spectra which are similar to those of other class II methanol transitions, for example at 6.7 GHz. Usually all the spectral features of the 107-GHz emission have counterparts in the 6.7-GHz spectra, although the 6.7-GHz spectra typically have more features than those at 107 GHz. The strongest 6.7-GHz features are as a rule also the strongest features in the 107-GHz spectrum, but there is no strong correlation between the flux density at the two frequencies. There are even strong 6.7-GHz masers which have not been detected at 107 GHz, for example 309.92+0.48 has a peak flux density of 635 Jy at 6.7 GHz but is less than 4.5 Jy (3−σ) at 107 GHz, and has been detected only with more sensitivity observations using SEST (Booth and Caswell, private communication).

The $0_0 - 1_{-1}E$ transition at 108 GHz is also a class II transition, and takes place between the $K = 0$ and $K = -1$ ladders, as do other methanol-E class II maser transitions: $2_0 - 3_{-1}E$ and $J_0 - J_{-1}E$ at 12.2 and 157 GHz, respectively. In comparison to the masers at 12 GHz and 157 GHz, 108-GHz masers are extremely rare. The only detected source is 345.01+1.79 (Val'tts 1998), which has a narrow (1.3 km s^{-1}) intense maser line blue-shifted from the wide thermal line. This has been confirmed by more sensitive Pico Veleta observations (Slysh et al. 1999c), and the two spectra of 345.01+1.79 can be seen on Fig. 6. The rest of sources detected at 108 GHz show only wide, apparently thermal emission lines.

It is well established that class II methanol masers are typically associated with ultracompact HII regions (Phillips et al. 1998; Walsh et al. 1997). The interpretation that the 107 and 108-GHz emission is produced by masing is supported by the results of statistical equilibrium calculations of

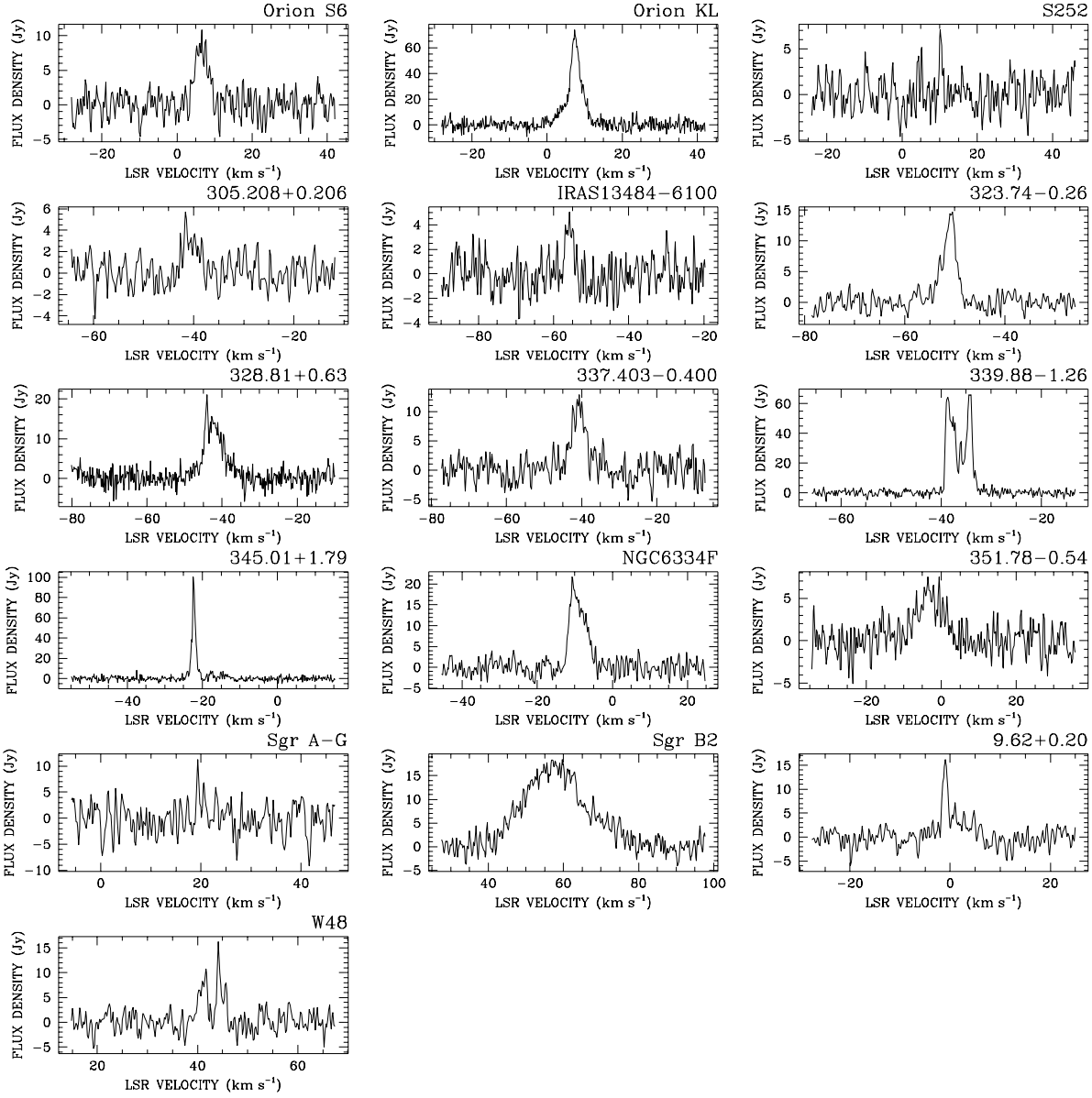

Figure 3. 107-GHz spectra. All spectra are Hanning smoothed, except for Orion KL, 328.81+0.63, 339.88-1.26 and 345.01+1.79

Table 5. Comparison of the observed flux densities and those calculated by LVG for 345.01+1.79

Transition	Frequency (GHz)	Observed flux density (Jy)	Calculated flux density (Jy)	Calculated optical depth
$5_1 - 6_0 A^+$	6.7	508	508	−8.2
$2_0 - 3_{-1} E$	12	310	340	−6.2
$3_0 - 4_1 A^+$	107	85.5	247	−2.4
$0_0 - 1_{-1} E$	108	9.5	109	−1.6
$4_0 - 4_{-1} E$	157	54.9	136	−1.6
$2_1 - 3_0 A^+$	157	21.4	112	−1.4

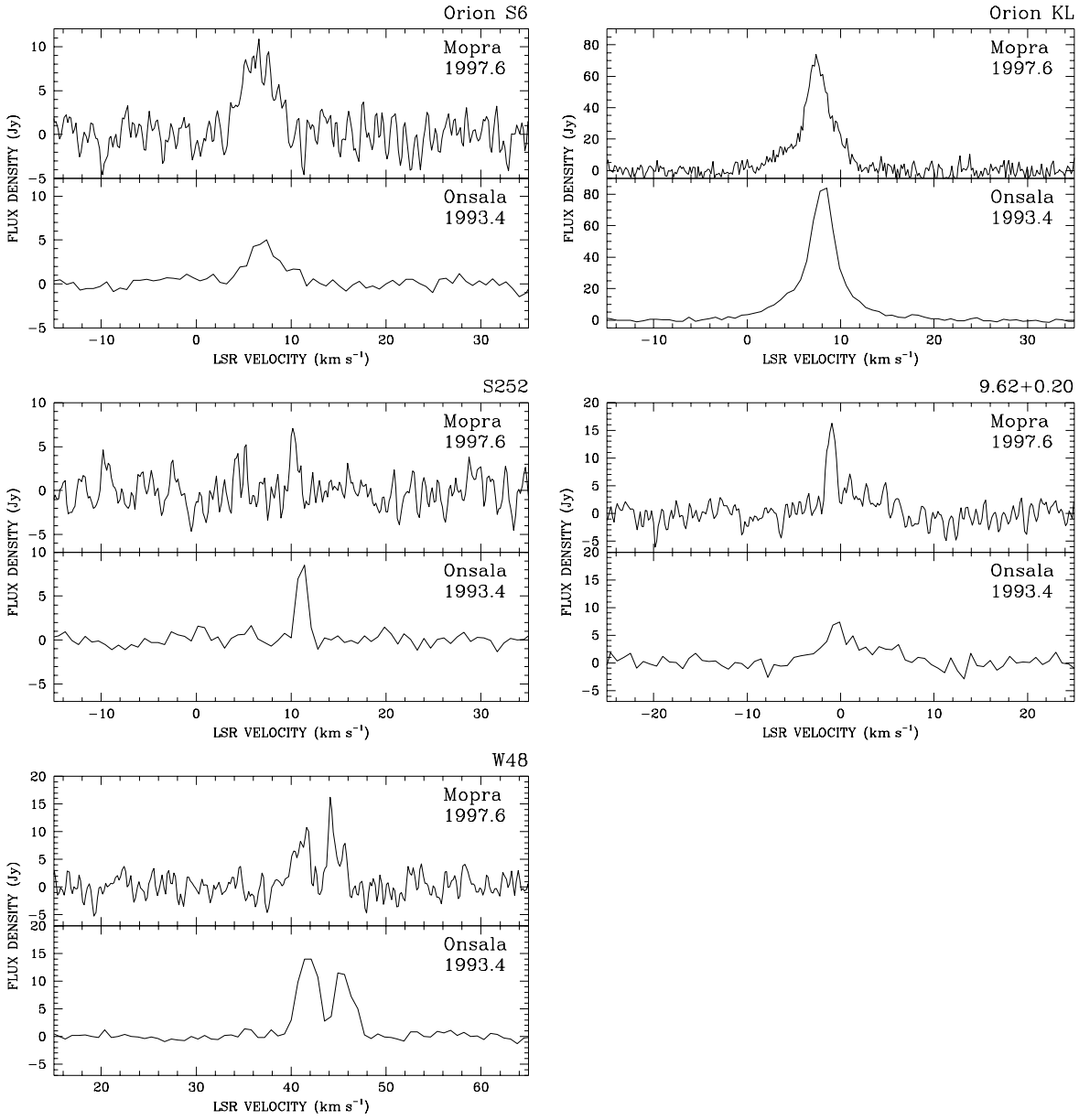

Figure 4. Comparison between Mopra and Onsala observations at 107 GHz.

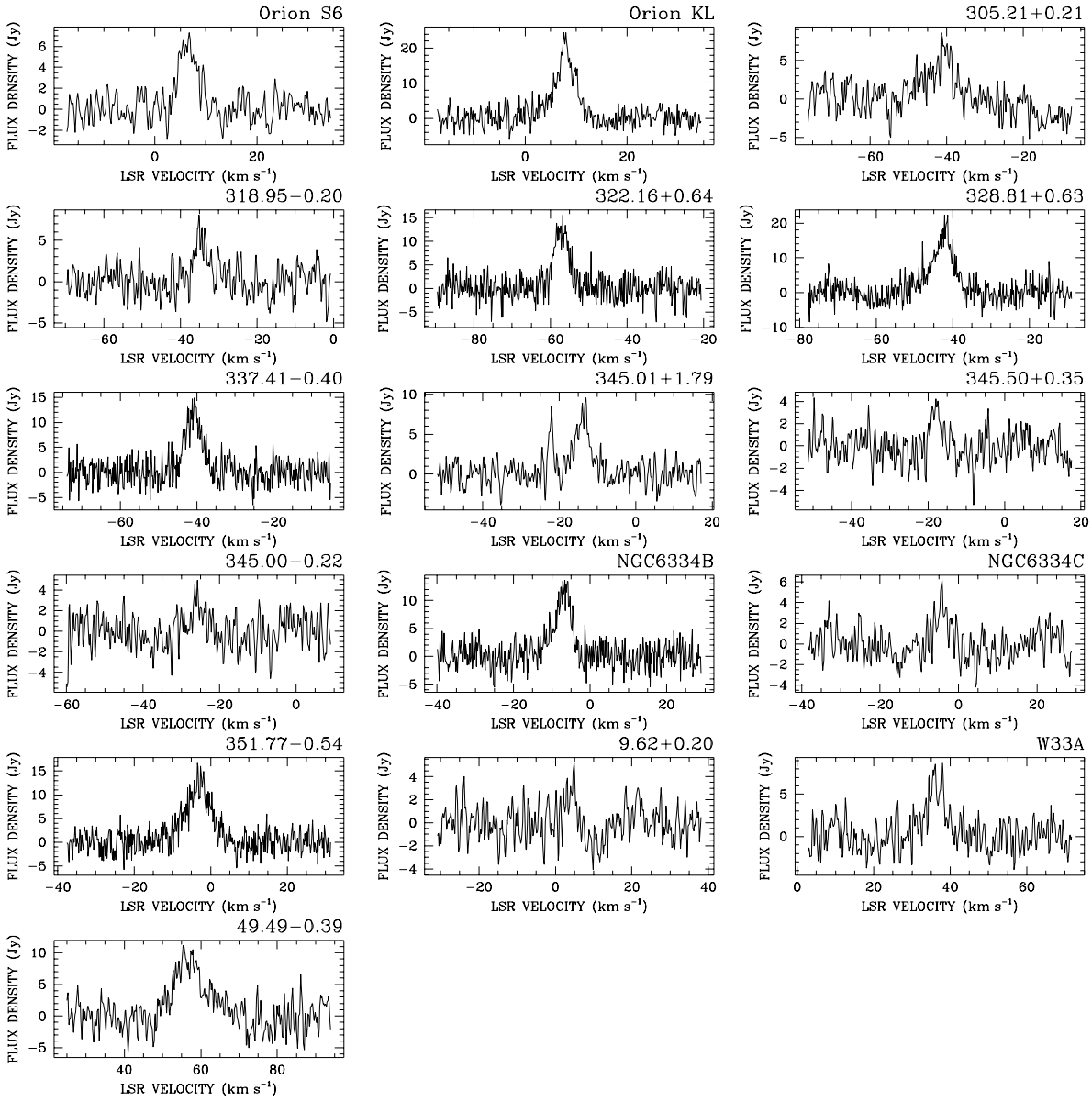

Figure 5. 108-GHz spectra. All spectra are Hanning smoothed, except for Orion KL, 322.16+0.64, 328.81+0.63, 337.41-0.40, NGC6334B and 351.77-0.54

methanol level excitation by external submillimeter/far infrared radiation from an ultracompact HII region, and deexcitation by collisions with cold gas particles. In Table 5 we present calculations of the relative intensity and optical depth of several class II methanol transitions. The observed and calculated flux densities in the strongest transition $5_1 - 6_0 A^+$ at 6.7 GHz were made equal. The modelling was performed with LVG code kindly supplied to us by Dr. Walmsley. The assumed molecular gas density was 10^7 cm^{-3}, temperature 50 K and methanol density divided by velocity gradient 0.5×10^{-1} cm^{-3} (km s^{-1} pc^{-1})$^{-1}$. The source was illuminated by a compact background HII region with an emission measure of 10^{12} cm^{-6}pc. The dilution factor was set to 0.2. The maser is excited by the combined action of the radiation from the compact HII region and collisions between methanol and hydrogen molecules. The collision selection rules employed in the model are based on the paper by Lees & Haque (1974) and imply that the $\Delta K = 0$ collisions are preferred.

All the transitions from Table 5 are inverted in our model. One can see in Table 5 a qualitative agreement between observed and calculated flux densities for all transitions; however, the quantitative agreement is good for the $2_0 - 3_{-1} E$ transition at 12 GHz, but at higher frequencies the calculated flux density is systematically higher by a factor 3 to 10. A more complicated model with regions of different temperature and density may well give a better agreement with observations. In addition, the required emission

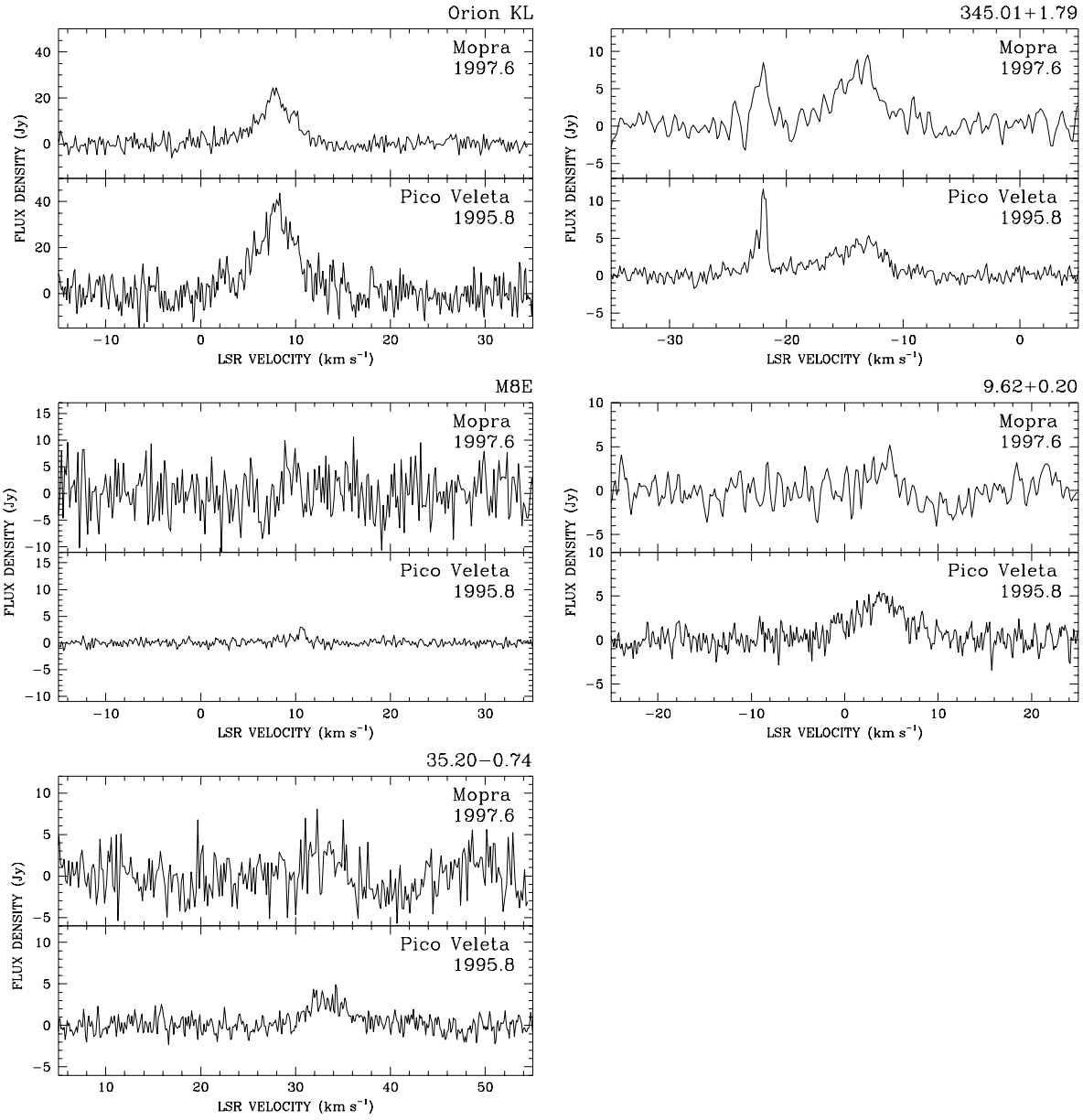

Figure 6. Comparison between Mopra and Pico Veleta observations at 108 GHz.

measure $EM = 10^{12}$ cm^{-6}pc seems to be too high, as no compact HII region with an emission measure of greater than 5×10^{10} cm^{-6}pc has been observed to date. Nevertheless, the qualitative agreement of the theory and observations for the $3_1 - 4_0A^+$ and $0_0 - 1_{-1}E$ transitions implies that both of them are class II methanol masers and that the maser emission in these transitions is excited by external radiation.

5 SUMMARY

1. As a result of a survey in the southern hemisphere 16 methanol emission sources were detected in the $3_1 - 4_0A^+$ transition at 107 GHz. This survey together with a similar survey made with the Onsala telescope completes a whole sky survey of methanol emission at 107 GHz.
2. Six new 107-GHz methanol masers were detected among 16 emission sources. Together with masers from the northern survey this makes a total of eleven 107-GHz methanol masers. They belong to class II.
3. A survey for methanol emission in the $0_0 - 1_{-1}E$ transition at 108 GHz has been carried out in the southern hemisphere with the detection of 16 new emission sources. One maser was found, also of class II.
4. The relative intensity of the class II methanol transitions is consistent with a maser model with radiative excitation and collisional de-excitation.

6 ACKNOWLEDGEMENTS

Authors are grateful to Dr. R. Booth and Dr. J. Caswell for communicating unpublished results from SEST observations at 107 GHz. I.E.V. is grateful to the ATNF for the hospitality, and to the staff of Mopra observatory for the help with the observations. The Australia Telescope is funded by the Commonwealth of Australia for operation as a National Facility managed by CSIRO. Travel to Australia for I.E.V. was aided by grant 96/1990 from the Australian Department of Industry, Science and Tourism. The work of I.E.V., V.I.S., S.V.K. and M.A.V. was partly supported by the grants 95-02-05826 and 98-02-16916 from the Russian Foundation for Basic Research. S.P.E thanks the Queen's trust for the computing system used to process the data from these observations.

REFERENCES

Batrla W., Matthews H.E., Menten K.M., Walmsley C.M., 1987, Nat., 326, 49
Bronfman L., Nyman L.A., May J., 1996, A&AS, 115, 81
Caswell J.L., Haynes R.F., Goss W.M., 1980, Aust. J. Phys., 33, 639
Caswell J.L., Gardner F.F., Norris R.P., Wellington K.J., McCutcheon W.H., Peng R.S., 1993, MNRAS, 260, 425
Caswell J.L., Vaile, R.A., Ellingsen, S.P., Whiteoak, J.B., Norris, R.P., 1995a, MNRAS, 272, 96
Caswell J.L., Vaile R.A., Ellingsen S.P., Norris R.P., 1995b, MNRAS, 274, 1126
De Lucia F.C., Herbst E., Anderson T., Helminger P., 1989, J. Mol. Spectr., 134, 395
Juvella M., 1996, A&AS, 118, 191
Kutner, M.L., Ulich, B.L., 1981, ApJ, 250, 341
Larionov G.M., Val'tts I.E., Winnberg A., Johansson L.E.B., Booth R.S., Golubev V.V., 1999, A&AS, submitted
Lees R.M., Haque S.S., 1974, Can. Journ. of Phys., 52, 2250
Mehringer D.M., Zhou S., Dickel H.R., 1997, ApJ, 475, L57
Menten K.M., 1991, In: Haschick A.D., Ho P.T.P.(eds.) Proc. Third Haystack Observatory Meeting, MA, USA, Skylines, 119
Menten K.M., 1991b, ApJ, 380, L75
Norris R.P., Caswell J.L., Gardner F.F., Wellington K.J., 1987, ApJ, 321, L159
Phillips C.J., Norris R.P., Ellingsen S.P., McCulloch P.M., 1998, MNRAS, 300, 1131
Schutte A.J., Walt D.J. van der, Gaylard M.J., MacLeod G.C., 1993, MNRAS, 261, 783
Slysh V.I., Kalenskii S.V., Val'tts I.E., Otrupcek R., 1994, MNRAS, 268, 464
Slysh V.I., Kalenskii S.V., Val'tts I.E., 1995, ApJ, 442, 668
Slysh V.I., Val'tts I.E., Kalenskii S.V., Larionov G.M., 1999a, Astron. Reports, in press
Slysh V.I., Val'tts I.E., Kalenskii S.V., Voronkov M.A., Palagi F., Tofani G., Catarzi M., 1999b, A&AS, 134, 115
Slysh V.I., Val'tts I.E., Kalenskii S.V., Voronkov M.A., 1999, in preparation
Smits D.P., 1994, MNRAS, 269, 11p
Val'tts, 1998, Astron. Letters, 24, 788
Val'tts I.E., Dzura A.M., Kalenskii S.V., Slysh V.I., Booth R.S., Winnberg A., 1995, A&A, 294, 825
Walsh A.J., Hyland A.R., Robinson G., Burton, M.G., 1997, MNRAS, 291, 261
van der Walt D.J., Gaylard M.J., MacLeod G.C., 1995, A&AS, 110, 81